Sādhanā (2020)45:241
https://doi.org/10.1007/s12046-020-01420-3

© Indian Academy of Sciences

Optimal two-stage parachute and retro motor sizing for launch vehicle stage recovery

PANKAJ PRIYADARSHI*, LEYA JOSEPH and KAMAL SAROHA

Vikram Sarabhai Space Centre, Trivandrum 695022, India
e-mail: pankaj_priyadarshi@vssc.gov.in

MS received 27 March 2019; revised 9 December 2019; accepted 14 February 2020

Abstract. A deceleration system consisting of staged parachute clusters and retro thrusters is optimized for the recovery of the first stage of a launch vehicle on sea. Optimal mass as well as reduction in speed by each parachute cluster and the retro thrusters is essential to minimize the inherent payload loss due to inclusion of additional systems. Three disciplines are involved in the study, namely parachute design, grain design and Three Degrees of Freedom (3-DOF) trajectory simulations. Parachute components are sized and their masses are estimated using a parachute design code. It computes the number of parachutes in the cluster, their sizes and opening loads for multiple reefing stages. Solid motor grain design is carried out, using high burn rate propellant, to provide high thrust to decelerate the launch vehicle stage to a near-zero descent rate at touchdown. A Multiobjective Multidisciplinary Design Optimization (M^2DO) problem has been formulated to minimize the mass of the deceleration system and minimize the touchdown speed of the recovered stage, subject to constraints on Maximum Expected Operating Pressure (MEOP), feasibility, etc. The optimization is carried out and the Pareto optimal front is obtained using an in-house multi-objective optimization algorithm, Attractor Anchored Multi-objective Evolutionary Algorithm (A^2-MOEA). A total of twenty-five design variables are considered including initial conditions for each deceleration stage, size of parachute cluster components for both drogue and main parachutes, and the size and shape of the solid motor grain for retro rockets. It is seen that the two objectives are conflicting. The Pareto optimal designs are discussed and the variation of design variables is presented.

Keywords. Multidisciplinary design optimization (MDO); multiobjective multidisciplinary design optimization (M^2DO); stage recovery; parachute cluster; solid motor grain design; three degrees of freedom (3-DOF) trajectory simulations; multi-objective evolutionary algorithm (MOEA); A^2-MOEA.

1. Introduction

Recovery of the booster stage of launch vehicles has been studied extensively for reducing the cost of access to space. The high energy of the stage has to be dissipated before its touchdown on land or sea. This is carried out typically by either using the vehicle propulsion or employing aerodynamic decelerators. For final stage of the recovery, hovering, impact attenuators and even mid-air recovery techniques have been studied. A high Technology Readiness Level (TRL) stage recovery system named Parachute-Retro-Float (P-R-F) is proposed, which employs multi-stage parachute clusters followed by retro thrusters for landing with near-zero touchdown speed in sea on floats. The parachute system consists of the drogue and main parachute clusters. The drogue parachute decelerates the payload to a speed suitable for the deployment of the main parachute, which reduces the speed of the payload to the desired terminal speed. The retro thrusters decrease the touchdown speed to the desired value before touching down in sea/land. It is essential to optimally size all the stages of the deceleration system together in order to reduce the total mass of the additional systems to ensure minimum payload loss.

Yang *et al* [1] carried out optimization of reef parameters to minimize the maximum instantaneous opening load during the operation of a multi-reefed parachute using Genetic algorithm. Leonard *et al* [2] proposed a probabilistic algorithm for the optimization of drogue-to-main transition altitude for high altitude, low opening ballistic air-drop. Brooks [3] carried out grain configuration optimization based on ballistic design analysis for a star grain. Though parachute-propulsion soft-landing technique is well known [4], Multiobjective Multidisciplinary Design Optimization (M^2DO) of the deceleration system has not been reported.

This paper discusses the design of the deceleration system consisting of multi-stage parachute clusters (both

*For correspondence
Published online: 19 September 2020

drogue parachute and main parachute) and the retro thrusters. The problem has been posed as a M^{2}DO problem to minimize the mass of the deceleration system while simultaneously minimizing the impact or touchdown speed. The aim is to obtain the Pareto optimal set of deceleration system components along with their sizing, which optimizes these two objectives.

In this paper we discuss the formulation of the M^{2}DO problem and the salient features of the Pareto optimal designs. Section 2 presents the methodology. Section 3 presents the optimal configurations and the variation of key design features. The conclusions are presented in Section 4.

2. Methodology

2.1 *Optimization problem formulation*

The M^{2}DO problem is posed in the Non-linear Programming Problem (NLP) form in Table 1, where $\vec{X}_{drogue}$, $\vec{X}_{main}$, $\vec{X}_{retro}$ refer to design variables of the drogue chute design, main chute design and the retro design disciplines, respectively. $\vec{X}_{coupling}$ represents the set of coupling variables. $\vec{X}_{min}$ and $\vec{X}_{max}$ refer to the lower and upper variable bounds, respectively. The first objective, f_1, of the optimization problem is to minimize the sum of the masses of the drogue parachute, the main parachute and retro motors (Eq.(1)). The second objective, f_2, is to minimize the touchdown speed (Eq. (2)). Eq. (3) and Eq. (4) quantify the feasibility or in-feasibility of a parachute system for a given set of design variables and fixed parameters. Occurrences like negative riser dimension, incompatible terminal state and reefing parameter, incompatible reefing fractions and disreef altitudes, and exceedance of maximum parachute diameter for a given maximum number of parachutes in a cluster constitute design in-feasibility. Eq. (5) checks for the existence of sustainable pressure inside the port volume for a given throat diameter. Eqs. (6) to (8) enforce constraints on Maximum Expected Operating Pressure (MEOP), grain port radius and nozzle exit diameter. All the objectives and the constraints are normalized.

The Individual Discipline Feasible (IDF) architecture has been employed in the present study to solve the Multidisciplinary Design Optimization (MDO) problem. A schematic of the M^{2}DO architecture is shown in Fig. 1. The set of twenty-five design variables ($\vec{X}$) is optimized. $\vec{X}$ is divided into three subsets, $\vec{X}_{drogue}$, $\vec{X}_{main}$ and $\vec{X}_{retro}$, which are given to the three disciplinary modules: drogue parachute, main parachute and grain design modules. Along with this a set of coupling variables, $\vec{X}_{coupling}$, is supplied by the optimizer to the disciplinary modules. The flow of design variables from the optimizer to the disciplinary analysis blocks is indicated by the blue arrows in Fig. 1. The constraint and objective function values are supplied back to the optimizer. This is indicated in green lines in the figure. The masses of the main parachute cluster and the retro motors are the coupling variables, which need to be fed back to the upstream modules. They are indicated below the modules along with dashed red lines. The estimated value of the coupling variables ($\vec{X}_{coupling} = \{m_{main,est}, m_{retro,est}\}$) is supplied by the optimizer to the disciplinary analysis blocks, which is used for the designs of drogue and main parachutes. The difference between the estimated values and the computed values of $\vec{X}_{coupling}$ is used as penalty, given as follows:

$$P = w_2(m_{main,est} - m_{main})^2 + w_3(m_{retro,est} - m_{retro})^2 + \Delta N_{lobe,int}. \quad (9)$$

The optimizer, Attractor Anchored Multi-objective Evolutionary Algorithm (A^2-MOEA), employs real-coded Genetic Algorithm (GA) and cannot handle integer design variables at present; hence the number of lobes in a star-grain is represented as a continuous design variable in the optimizer, and a penalty equal to the square of difference between its value and its rounded off value ($\Delta N_{lobe,int}$) is also added in Eq. (9). The penalty P is added to the first

Table 1. The M^{2}DO problem

minimize	$f_1 : m_{drogue} + m_{main} + m_{retro} + P$	(1)
$(\vec{X})$	$f_2 : V_{touchdown}$	(2)
$\vec{X}$	$= \{\vec{X}_{drogue}, \vec{X}_{main}, \vec{X}_{retro}, \vec{X}_{coupling}\} \in [\vec{X}_{min}, \vec{X}_{max}]$	
subject to:		
	$g_1 : \Delta_{drogue} \geq 0$	(3)
	$g_2 : \Delta_{main} \geq 0$	(4)
	$g_3 : \Delta_{retro} \geq 0$	(5)
	$g_4 : 10^7 - MEOP \geq 0$	(6)
	$g_5 : D_{e,max} - D_e \geq 0$	(7)
	$g_6 : r_p - 20.0 \geq 0$	(8)

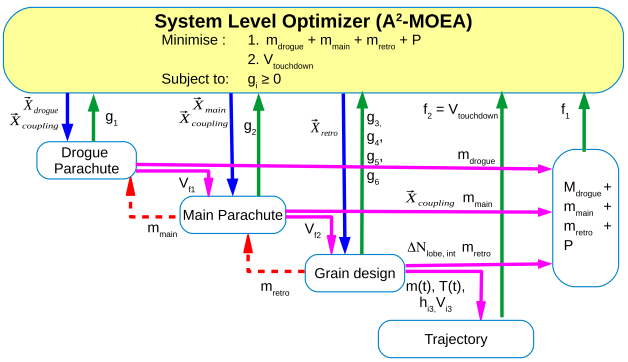

Figure 1. Architecture of the M^{2}DO problem.

objective to ensure convergence of the coupling variables and the number of lobes.

The first three modules in Fig. 1 contribute to the computation of the first objective function, f_1, and all six constraints, g_1–g_6. The inputs from the grain design module go to the trajectory module, which evaluates the second objective function, f_2. The terminal Equivalent Air Speed (EAS) of the drogue parachute, $\mathcal{V}_{f_1}$, goes as an input to the main parachute design module as initial speed, $\mathcal{V}_{i_2}$. Similarly, the terminal EAS of the main parachute, $\mathcal{V}_{f_2}$, goes as an input to the trajectory simulation module as $\mathcal{V}_{i_3} = \mathcal{V}_{f_2}$ along with the retro thrust ($T(t)$) and propellant mass, $m_p(t)$. The trajectory code initiates the firing of the retro motor at an altitude of h_{i_3}, which is also a design variable.

The design variable subsets $\vec{X}_{drogue}$ and $\vec{X}_{main}$ include suspension line length to nominal diameter ratio (L_e/D_0), forebody distance from parachute, reefing fraction, disreef altitude, terminal equivalent speed and terminal altitude. The deployment altitude for the drogue parachute is fixed; however, $\vec{X}_{main}$ also includes parachute deployment altitude in addition to the design variables listed for the drogue chute. $\vec{X}_{retro}$ includes retro ignition altitude and the grain design variables, namely outer diameter, length, port radius, slot tip height, slot base thickness, slot radius, ratio of port to nozzle throat areas, nozzle area ratio and number of lobes of grain. Initial state of drogue parachute deployment, body parameters, design factors and materials of parachute components, number of retro thrusters, nozzle half angle, bounds and other tolerances on various factors are fixed parameters for the problem.

2.2 *Parachute cluster design (Parachute Design and Analysis Code (ParDAC))*

Parachute Design and Analysis Code (ParDAC) is an in-house code that designs parachute clusters to achieve a user-specified terminal condition from its state of deployment. When the parachute achieves terminal velocity, total weight of the parachute-body system is balanced by the total drag on the system. Hence, nominal diameter of the parachute is calculated via a force balance along the vertical direction. The drag coefficient of a parachute is dependent on a number of parameters like the shape of the canopy, rate of descent, the wake effect due to forebody, interference effect due to clustering of parachutes and so on. The experimental results presented by Knacke [5] are used to account parachute drag coefficient (C_{D_0}) as a function of rate of descent, the ratio of suspension line length to nominal diameter of parachute (L_e/D_0) and number of parachutes. Hence, drag coefficient with respect to nominal area (S_0) of the parachute is computed as

$$C_{D_0} = C_{D_{0_{rod}}} \times \mathcal{F}C_{D_{0,\frac{L_e}{D_0}}} \times \mathcal{F}C_{D_{0,N}} \tag{10}$$

where $C_{D_{0_{rod}}}$ is C_{D_0} at the user-defined rate of descent, $\mathcal{F}C_{D_{0,\frac{L_e}{D_0}}}$ is a factor indicating the drag augmentation due to increase in $\frac{L_e}{D_0}$ and $\mathcal{F}C_{D_{0,N}}$ is a factor quantifying drag reduction due to parachute clustering.

Parachute opening force during each reefing stage is calculated using canopy loading (W/C_DS) method proposed by Knacke [5], the drag area variation during parachute inflation proposed by Yang *et al* [1] and the trajectory simulator described in Section 2.4. For a multi-reefed parachute, the drag area variation during its inflation to the first reefed configuration can be assumed to be linear with time, while the inflation following further disreefing is assumed to be exponential with time. Following [1], the variation of drag area (C_DS) with time is taken as follows:

$$C_DS = \begin{cases} \dfrac{(C_DS)_1}{t_p}\, t, \quad (0 \le t \le t_p) \\ (C_DS)_1, \quad (t_p \le t \le t_{y_1}) \\ (C_DS)_1 + \left[(C_DS)_2 - (C_DS)_1\right]\left(\dfrac{t - t_{y_1}}{t_{m1}}\right)^{\eta,1}, \\ \qquad (t_{y_1} \le t \le t_1) \\ \vdots \\ (C_DS)_n, \quad (t_{n-1} \le t \le t_{n-1} + t_{y_n}) \\ (C_DS)_n + \left[(C_DS)_{n+1} - (C_DS)_n\right]\left(\dfrac{t - t_{y_n} - t_{i-1}}{t_{mn}}\right)^{\eta,n}, \\ \qquad (t_{n-1} + t_{y_n} \le t \le t_n) \end{cases} \tag{11}$$

where t_p, t_y and t_m represent pre-inflation time, reefed time of a canopy reefing stage and filling time of a reefed stage, respectively.

During inflation to the first reefed stage, opening force is given by Knacke [5] as follows:

$$F_i = \begin{cases} (C_DS)_1\ q\ C_X\ X \\ \left[(C_DS)_i - (C_DS)_{i-1}\right]\ q\ C_X\ Xi = 2, 3\ldots \end{cases} \tag{12}$$

where C_X and $\vec{X}$ refer to opening force coefficient at infinite mass (encountered in wind tunnel tests in which velocity reduction due to parachute is not achieved) and force reduction factor to incorporate the finite mass condition, respectively. In case of disreefing, opening force depends on the change in drag area during disreefing. The subscript i refers to the number of reefing stage for which opening load is calculated. C_DS in Eq. (12) is obtained from reefing fractions that are design variables in optimization and the computed value of drag area of the designed parachute after complete inflation. Also, q at disreef altitudes is obtained from trajectory computations.

The maximum opening load (F_{max}) among the various F_i is used for component sizing and mass estimation of various components. The design loads for canopy (μ_{lcnpy}), suspension lines (μ_{susp}), radial lines (μ_{rad}), vent lines (μ_{vline}), skirt band (μ_{sband}) and riser (μ_{riser}) with Design Factor (DF) are as follows:

$$\mu_{lcnpy} = \frac{F_{max} \times DF_{cnpy}}{\pi \times (D_p)} \tag{13}$$

$$\mu_{susp} = \frac{F_{max} \times DF_{susp}}{n_{susp}} \tag{14}$$

$$\mu_{rad} = \frac{F_{max} \times DF_{susp}}{n_{susp}} \tag{15}$$

$$\mu_{vline} = \frac{F_{max} \times DF_{susp}}{n_{susp}} \tag{16}$$

$$\mu_{sband} = 0.05F_{max} \times DF_{sband} \tag{17}$$

$$\mu_{riser} = NF_{max} \times DF_{riser}. \tag{18}$$

The number of material layers for the components is then decided using the material strength, followed by mass estimation.

2.3 *Ballistic Incremental Analysis Code (BINC)*

The Ballistic Incremental Analysis Code (BINC) evaluates the thrust time profile, pressure time profile and other characteristics of the solid motor grain. It is implemented as a C++ class to estimate the quantities required for the MDO study. For a given grain geometry, first the burning surface area of the grain and the port area are computed as a function of web thickness. The burn rate of the propellant is used to calculate the mass and energy flux into the control volume at a given time. Burn rate augmentation due to the flow properties is also accounted. Conservations of mass, momentum and energy along with experimentally obtained flame properties are employed to compute the one-dimensional flow inside solid motor. The pressure is iterated to convergence while accounting for the mass ejected through the nozzle. The module computes the vacuum thrust, propellant mass and nozzle exit properties as a function of time. The overall flow of the BINC is shown in Fig. 2.

The grain geometry evolution is estimated as a function of web thickness. This is accomplished using geometrical and analytical relations to get the exact perimeter and surface area of a particular grain. The grain geometry is decided based on the six design variables: grain outer dimeter, port_radius, slot tip height, slot base thickness, slot radius and number of lobes. This parameterization of the grain geometry results in five different types of grains, namely slot-star with port, slot star, dimple star with port, dimpled star and cylindrical. In addition to the above six design variables, the grain length and the nozzle area ratio are the other propulsion related design variables.

The computational domain, depicted in Fig. 3, consists of a number of sections divided along the length. One-dimensional analysis is carried out and the gas state is estimated along the length of the grain. A database of the exposed surface area with constant increments in web thickness is calculated by BINC. It is used to estimate the surface area at any location and at any web thickness. The following assumptions are employed in order to estimate the pressure–thrust signature of the solid rocket motor (SRM):

- Quasi steady 1-D analysis is carried out and no initial and final transients are computed.
- Velocity at head end of the SRM is taken as zero.
- No erosive burning is considered at the head end, as velocity is taken as zero.
- The flow is assumed to be choked at the nozzle throat.
- Ideal gas approximation for the combustion products is used.
- Available experimental data has been employed for the throat degradation factor, burn rate augmentation factors and the flame properties.
- Mukunda model [6] is used to account for erosive burning.
- For the CG calculation, the section CG is assumed to be at the centre of the section.
- Flame properties, the flame temperature, C^*, Prandtl number, density, molecular weight, ratio of specific heats and absolute viscosity are only pressure dependent.
- Thrust is assumed to be non-significant if the chamber pressure falls below 0.7 bar.

During the analysis, the burn rate of the propellant at a given section is estimated using the Saint Roberts law as a function of pressure of the gases at that section. It is used to calculate the mass and energy flux fed into the control volume (section) at a given time. The burn rate is also used to calculate the incremental change in exposed surface area and port area at the next time step. The one-dimensional conservation of mass, momentum and energy equations along with experimentally obtained flame properties are employed to compute the special gradients of the pressure, temperature and density of gases. Burn rate augmentation due to the erosive burning is also accounted. The pressure is iterated to convergence to satisfy the 1-D conservation principals of the flow inside the SRM at a given time. Finally, the module computes the vacuum thrust, propellant mass and nozzle exit properties for a converged chamber pressure as a function of time.

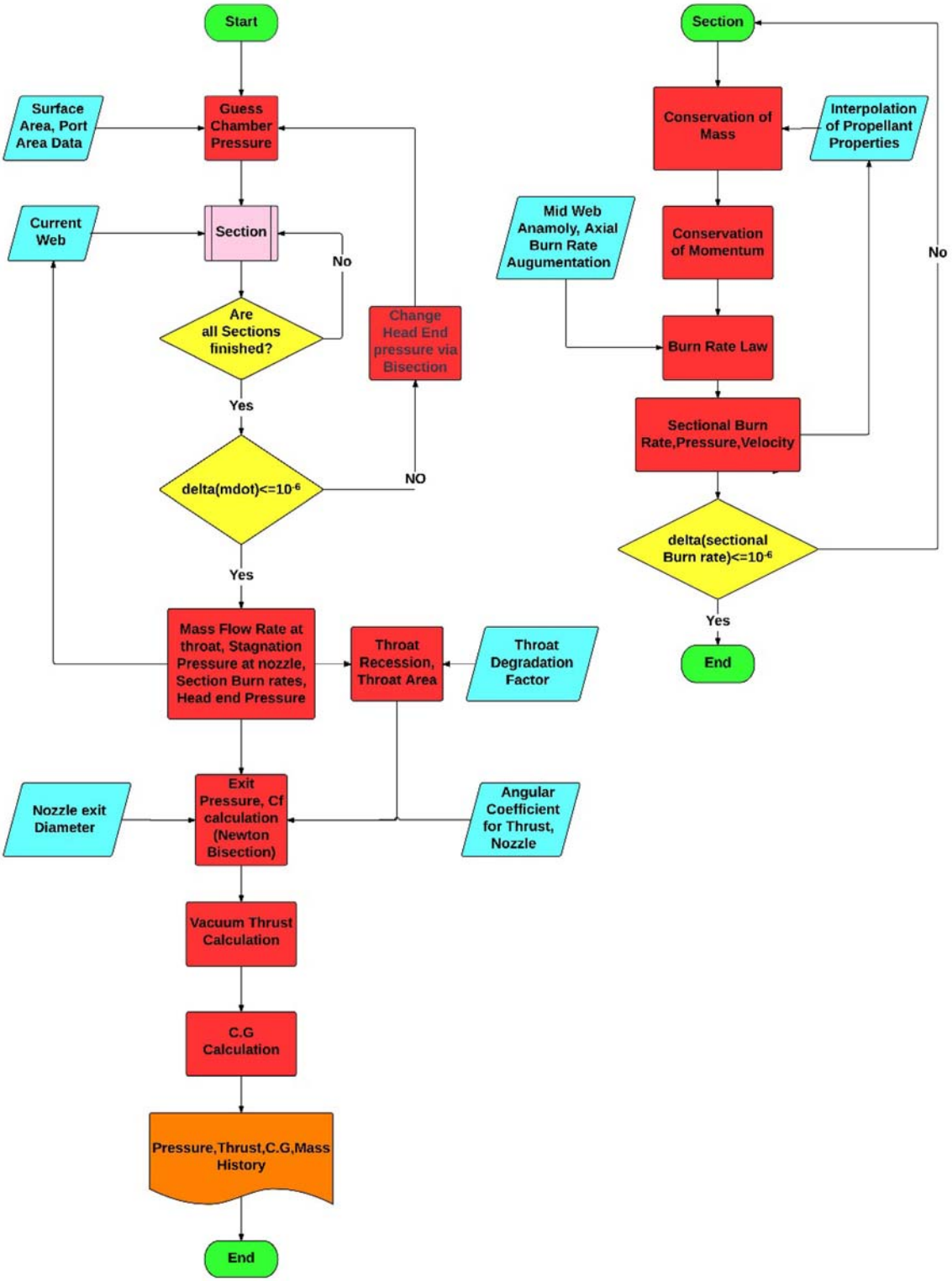

Figure 2. Flow chart of the algorithm employed in BINC.

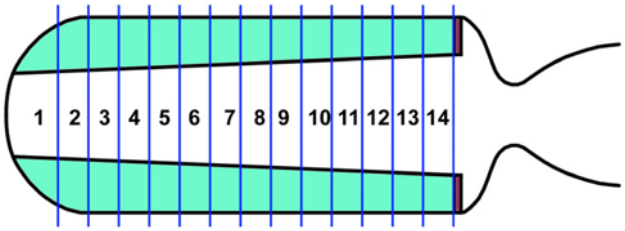

Figure 3. Schematic of a rocket motor with its grain divided into small elements.

2.4 *Three Degrees of Freedom (3-DOF) Trajectory Code*

The 3DOF equations are given in earth-centred rotating spherical co-ordinate system $\{r, \theta, \phi\}^T$, where r is the distance from the centre of earth, θ is the longitude and ϕ is the latitude (Fig. 4). The velocity is specified in terms of its magnitude (V), the flight path angle (γ) and the heading angle (ψ). The heading angle (ψ) is defined with respect to the local East in Velocity Aligned Reference Frame (VARF) (Fig. 5). First the three kinematic equations are listed, followed by the three dynamic equations:

$$\dot{r} = V \sin(\gamma) \tag{19a}$$

$$\dot{\theta} = \frac{V \cos(\gamma)\ \cos(\psi) - r\ \cos(\phi)\, \omega_{E,I}}{r\ \cos(\phi)} \tag{19b}$$

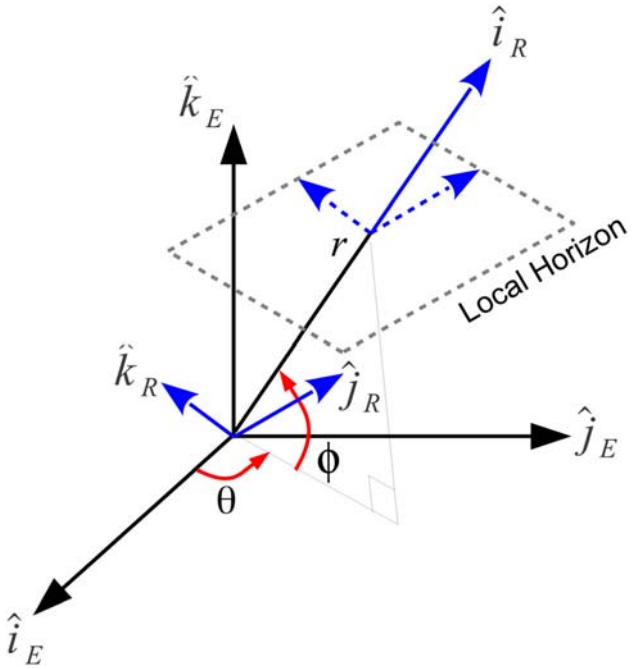

Figure 4. Radius Aligned Reference Frame (RARF)

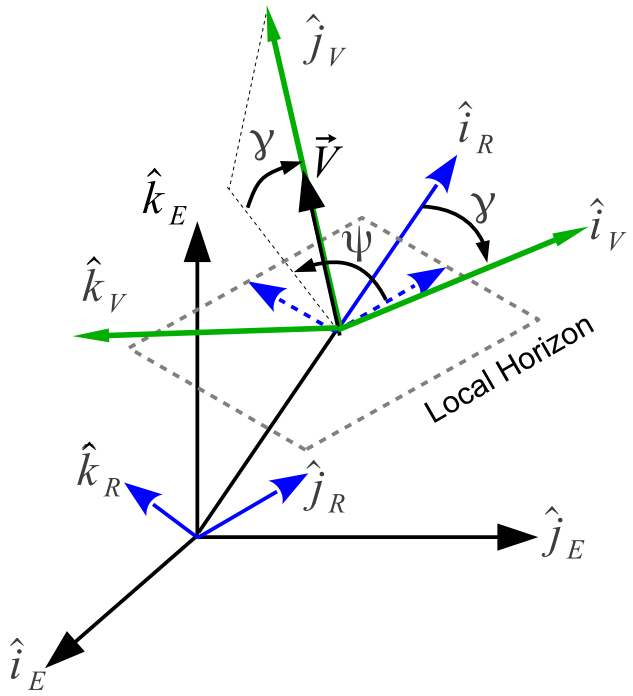

Figure 5. Velocity Aligned Reference Frame (VARF)

$$\dot{\phi} = \frac{V \cos(\gamma)\ \sin(\psi)}{r} \tag{19c}$$

$$\begin{aligned} \dot{V} = &-\frac{D}{m} + \omega_{E,I}^2 r \cos^2(\phi)\big(\sin(\gamma) \\ &- \cos(\gamma)\tan(\phi)\sin(\psi)\big) + \frac{T_V}{m} \end{aligned} \tag{19d}$$

$$\begin{aligned} V\dot{\gamma} = &-\frac{L}{m}\cos(\sigma) - g\cos(\gamma) + \frac{V^2}{r}\cos(\gamma) \\ &+ 2\omega_{E,I} V \cos(\phi)\cos(\psi) \\ &+ \omega_{E,I}^2 r \cos^2(\phi)\big(\cos(\gamma) + \sin(\gamma)\tan(\phi)\sin(\psi)\big) \\ &- \frac{T_L}{m}\cos(\sigma_T) \end{aligned} \tag{19e}$$

$$\begin{aligned} V\dot{\psi} = &\frac{L}{m}\frac{\sin(\sigma)}{\cos(\gamma)} - \frac{V^2}{r}\cos(\gamma)\cos(\psi)\tan(\phi) \\ &+ 2\omega_{E,I} V\big(\tan(\gamma)\cos(\phi)\sin(\psi) - \sin(\phi)\big) \\ &- \frac{\omega_{E,I}^2 r \sin(\phi)\cos(\phi)\cos(\psi)}{\cos(\gamma)} \\ &+ \frac{T_L}{m}\frac{\sin(\sigma_T)}{\cos(\gamma)} \end{aligned} \tag{19f}$$

In these equations, D is the drag, L is the lift and T is the thrust. The thrust is resolved into two mutually orthogonal components – a component T_V along the positive velocity direction and the other component T_L perpendicular to it:

$$T_V = T\ \cos\theta_T, \tag{20}$$

$$T_L = T\ \sin\theta_T. \tag{21}$$

Here, θ_T is the angle between the thrust vector and the velocity vector. The lift bank angle is denoted by σ and on similar lines, σ_T denotes the thrust bank angle. The $\omega_{E,I}$ is the angular velocity of earth with respect to an Earth Centered Inertial (ECI) reference frame. The mass m is a variable that changes due to the change in propellant mass ($\dot{m}$). The propellant mass flow rate can be computed using the specific impulse of the rocket, I_{SP}, as follows:

$$\dot{m} = \frac{T}{I_{SP}}. \tag{22}$$

The trajectory code is implemented as a class in C++ language. The initial state vector, $\vec{s} = \{r, \theta, \phi, V, \gamma, \psi\}$ is specified and these six equations are integrated using the RK-4 method. The spherical earth gravitational model has been used along with a standard atmosphere model with a non-rotating earth.

2.5 *Attractor Anchored Multi-objective Evolutionary Algorithm (A^2-MOEA)*

In the current study we have used Attractor Anchored Multi-objective Evolutionary Algorithm (A^2-MOEA) [7], a real-coded GA-based Multi-objective Evolutionary Algorithm (MOEA). For n_f-dimensional objective space, the algorithm defines attractors in the space of first $n_f - 1$ dimensions. In the selection operator of A^2-MOEA, the solutions that are closest to these attractors are preferred over other solutions and are designated as *Elite*, which survive over GA generations. This ensures more uniform spread and better convergence of the Pareto front.

3. Results

The M^{2}DO problem was solved for the recovery of spent rocket stage descending at an initial speed of 150 m/s at an altitude of 7 km. Three cases were considered, having spent stage masses of 4000, 8000 and 12000 kg. Population sizes of 140 and 250 were used for running A^2-MOEA. Results of the optimization problems are presented in the form of Pareto fronts with *X*-axis representing the first design objective, the *Y*-axis representing the second design objective and the colour of the symbols representing the value of a third variable (Fig. 6). It can be seen that the two objectives are conflicting, i.e. reduction in terminal speed requires higher mass and vice versa.

From the results (e.g., Fig. 6a) it can be observed that the Pareto front can be divided into three regions: Region R1, where the terminal speed is high and the deceleration system employs only the drogue parachute; Region R2, where the terminal speeds are intermediate and the deceleration is provided by both the drogue parachute and the main parachute clusters; Region R3, where the terminal speeds are low and retro propulsion is employed to reduce the terminal speed in addition to use of the drogue and main parachutes (Fig. 6b).

This is because it is efficient to reduce the speed using parachutes for higher terminal speeds, where dynamic pressure is significant. As the mass of the parachute is inversely proportional to the square of the terminal speed, the terminal speed reduction using parachute becomes inefficient at low terminal speeds. This is seen from the results, where the terminal speed becomes relatively flat in the end of R2 region as a consequence of the large rise in main parachute diameter to reduce the terminal speed. However, the mass of propellant for a given ΔV is independent of the terminal speed. Therefore, at low terminal speeds, the optimizer configures a deceleration system that first employs parachutes followed by a retro motor to decelerate the stage. The slope of the Pareto front in region R3 becomes steeper as spent stage mass reduces, indicating diminishing advantage of retro system in impact speed reduction with increase in spent stage mass. The clear demarcation of regions R1, R2 and R3 indicates that the optimization problem considered has variable dimension in design variable space.

With increase in the spent stage mass, for a given terminal speed, the optimal deceleration system mass increases in all three regions, e.g., in region R3, larger retro motor is required to retard a heavier stage (Fig. 6b). Similarly, for a given mass of the deceleration system, the terminal speed increases with increase in spent stage mass. For a given spent stage mass, the size of drogue parachute increases with reduction in terminal speed in the region R1 (Fig. 6c).

However, the drogue size is not sensitive to change in the terminal speed in the regions R2 and R3. Similarly, the size of main parachute rises with reduction in touchdown speed in region R2 (Fig. 6d). In region R3, the propulsion starts contributing while the main parachute reduces to a nearly constant size. The retro mass increases with the decrease in terminal speed. Transition between second and the third regions is influenced by the maximum allowable diameter of a parachute ($D_{0,max}$ =38 m) in cluster, which is a fixed parameter. The optimal design shifts from having no main parachute in R1 to systems with one, two or three main parachutes in R2 (Fig. 6a), and further to a single main parachute in R3.

The decrease in terminal speed in regions R1 and R2 leads to increase in the maximum opening loads on both drogue and main parachutes (Fig. 6e, f) due to increase in parachute size. The opening loads also increase significantly with increase in stage mass. Both the drogue and the main parachutes are reefed.

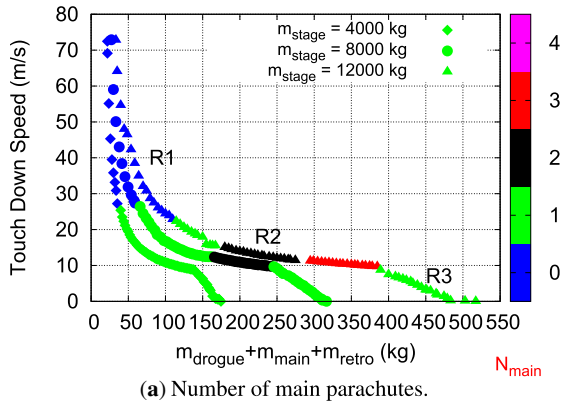

(**a**) Number of main parachutes.

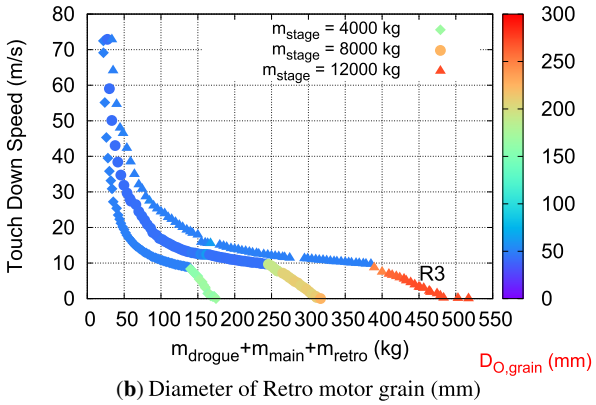

(**b**) Diameter of Retro motor grain (mm)

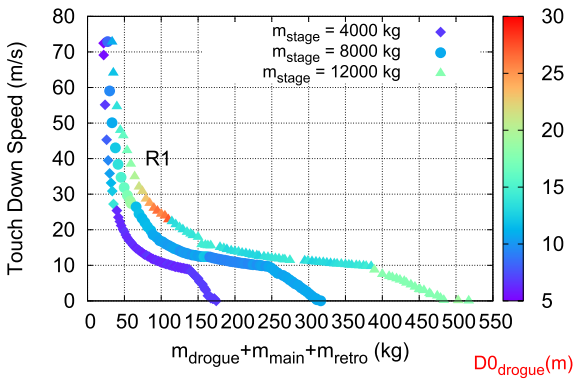

(**c**) Diameter of drogue parachute (m)

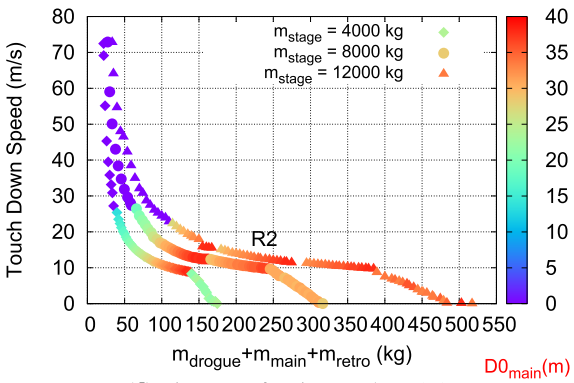

(**d**) Diameter of main parachute (m)

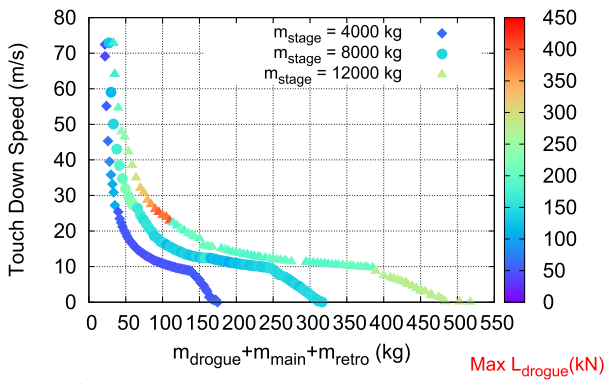

(**e**) Maximum opening load on drogue parachute (kN)

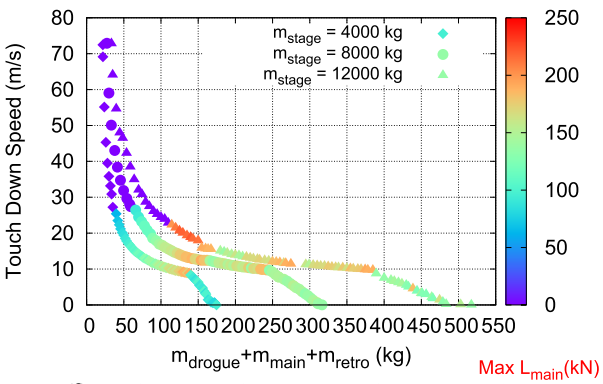

(**f**) Maximum opening load on main parachute (kN)

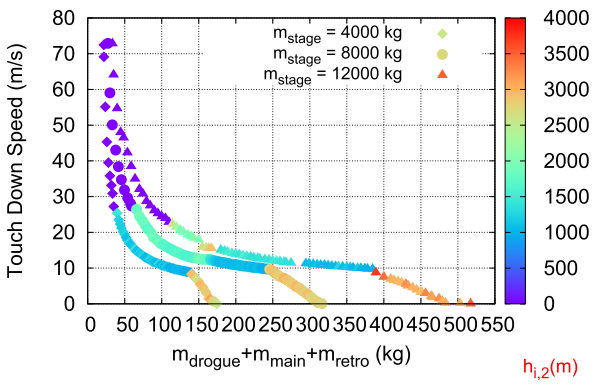

(**g**) Deployment altitude of main parachute (m)

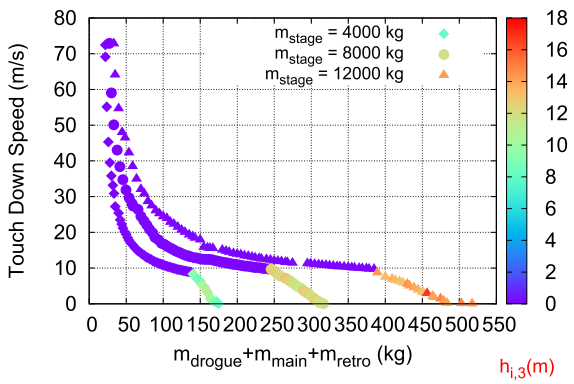

(**h**) Altitude for retro motor ignition (m)

Figure 6. Results of deceleration system M^{2}DO for recovery of 4000, 8000 and 12000 kg stages.

The reefing ratios and disreef altitudes for the drogue and the main parachutes have been optimized along with the deployment altitude of the main parachute and the ignition altitude for the retro motors. The optimal deployment altitude for the main parachute is shown in Fig. 6g and the optimal retro motor ignition altitude is shown in Fig. 6h. It is seen that when the terminal speeds are lower than ≈10 m/s (region R3) the deployment altitude of the main parachute jumps to significantly higher altitudes along with a lower size of main parachute, as discussed earlier (Fig. 6d). It may be noted that lower size main parachutes, in the region R2, are also deployed at higher altitudes. The optimal ignition altitude for the retro motor is very small in all cases, 8–18 m in the present case, and does not vary significantly with decrease in terminal speed. The optimal ignition altitude increases with increase in the spent stage mass, as expected.

4. Conclusions

The design of a deceleration system for stage recovery has been posed as an M^{2}DO problem. The deceleration system two-stage parachutes (with reefing) and a retro motor. Two parachute design modules (for design of drogue and main parachute clusters), a retro motor design module and a trajectory module have been implemented for this multidisciplinary design optimization problem. Two conflicting objectives, namely the mass of the deceleration system and the touchdown speed, are minimized together, subject to constraints in parachute design and retro motor design while considering twenty-five design variables.

The optimal design set divides into three distinct subsets. First subset: the optimal deceleration system for touchdown speeds larger than ≈ 25 m/s consists only of drogue parachutes; second subset: for touchdown speeds between ≈10 and 25 m/s, the optimal design solution consists of only drogue and main parachutes and third subset: for terminal speeds below ≈10 m/s, it is optimal to have drogue parachutes with retro motors and less number of main parachutes. Another interesting observation is that the size of drogue parachutes is insensitive to the desired touchdown-speed for the second and third subsets. Therefore, the present M^{2}DO study is able to discover broad design rules for this multidisciplinary design problem.

Thus depending on the impact speed of interest, the recovery system design optimization can be simplified by choosing the optimal deceleration system constituents which would reduce the number of design variables for regions R1 and R2.

The masses of drogue parachute, main parachute and retro motor systems increase with decrease in terminal speed in the regions where these systems dominate the deceleration of the stage. The optimal variation of various paramaeters related to the parachute and retro motor deceleration phases have been discussed.

Nomenclature

Acronyms

3-DOF	Three Degrees of Freedom
A^2-MOEA	Attractor Anchored Multi-objective Evolutionary Algorithm
BINC	Ballistic Incremental Analysis Code
CG	Center of Gravity
DF	Design Factor
EAS	Equivalent Air Speed
ECI	Earth Centered Inertial
GA	Genetic Algorithm
IDF	Individual Discipline Feasible
M^{2}DO	Multiobjective Multidisciplinary Design Optimization
MDO	Multidisciplinary Design Optimization
MEOP	Maximum Expected Operating Pressure
MOEA	Multi-objective Evolutionary Algorithm
NLP	Non-linear Programming Problem
P-R-F	Parachute-Retro-Float
ParDAC	Parachute Design and Analysis Code
TRL	Technology Readiness Level
VARF	Velocity Aligned Reference Frame

Greek symbols

ϕ	Elevation Angle, Latitude (rad)
γ	Flight Path Angle (rad)
θ	Longitude (rad)
θ^T	Angle between thrust vector and the velocity vector (deg)
ω	Angular Velocity (rad/s)
ψ	Heading Angle (rad)
σ	Bank Angle for lift (deg)
σ^T	Bank Angle for thrust (deg)
η	Opening profile shape exponent
μ	Design load
μ^l	Design load per unit length

Other symbols

C_DS	Drag area
C_{D_0}	Drag coefficient defined with respect to area corresponding to nominal diameter
$C_{D_{0,\,ROD}}$	C_{D_0} at a particular rate of descent
C_X	Opening force coefficient at infinite mass (dimensionless)
D	Diameter
D_0	Nominal diameter
$D_{0,max}$	Maximum allowable diameter of a parachute in a cluster
D_e	Nozzle exit diameter

$\Delta N_{lobe,int}$	Penalty for non-integer value of the number of lobes
$\mathcal{F}C_{D_{0,\frac{Le}{D_0}}}$	Factor indicating drag augmentation due to increase in $\frac{Le}{D0}$. It is 1 when $\frac{Le}{D0} = 1$
$\mathcal{F}C_{D_{0,N}}$	Factor indicating drag reduction due to parachute clustering. It is one when number of parachutes in cluster is 1
$\mathcal{V}$	Equivalent Air Speed
Δ_{retro}	Indicates feasiblity of sustainable combustion inside the retro motors
Δ_{drogue}	Indicates feasibility of a parachute design
Δ_{main}	Indicates feasibility of a parachute design
$D_{e,max}$	Maximum nozzle exit diameter
D_p	Projected diameter of parachute
F	Opening load
h	Height, m
I_{SP}	Specific Impulse, Ns/kg
L	Length
L_e	Length of suspension line
m	Mass, kg
$\dot{m}$	Mass flow rate of propellant (kg/s)
C^*	Characteristic velocity of the propellant
n_f	Number of objective functions
n_{susp}	Number of suspension lines
P	Penalty
q	Dynamic Pressure
r_p	Grain port radius
r	Radius (m)
S_0	Reference area corresponding to D_0. $S_0 = \frac{\pi D_0^2}{4}$
$\vec{s}$	The state vector $\vec{s} = \{r, \theta, \phi, V, \gamma, \psi\}$
T	Thrust, N
t	time, s
t_m	Filling time of a reefed stage
t_p	Pre-inflation time
t_y	Reefed time of a canopy reefing stage
T_L	Component of thrust along vehicle lift (N)
T_V	Component of thrust along vehicle velocity (N)
V	Speed (m/s)
W	Weight carried by canopy
w	weight
$\vec{X}$	Design Variable
X	Force reduction factor (dimensionless)

Subscripts

1	For drogue parachute
2	For main parachute
3	For retro firing
cnpy	Canopy
coupling	coupling
drogue	Drogue parachute
est	Estimated
f	Terminal
i	Initial
main	main parachute
max	Maximum value
p	Propellant
rad	Radial line
retro	retro rocket
riser	Riser
sband	Skirt band
susp	Suspension line
vline	Vent line

References

[1] Xue Y, Yu L and Zhao X S 2017 Optimization of the reefed parachute using genetic algorithm. *Engineering Computations* 34.6 (2017): 1923–1938.

[2] Leonard A *et al* 2017 Probabilistic algorithm for ballistic parachute transition altitude optimization. *Journal of Guidance, Control, and Dynamics* (2017): 1–13.

[3] Brooks W T 1982 Ballistic optimization of the star grain configuration. *Journal of Spacecraft and Rockets* 19.1 (1982): 54–59.

[4] Harrison E F and Slocumb Jr T H 1969 Evaluation of entry and terminal deceleration systems for unmanned Martian landers. *Journal of Spacecraft and Rockets* 6.10 (1969): 1109–1113.

[5] Knacke T W 1991 *Parachute recovery systems design manual*. No. NWC-TP-6575, Naval Weapons Center China Lake, CA.

[6] Mukunda H S and Paul P J 1997 Universal behavior in erosive burning of solid propellants. *Combustion and Flame*, vol. 109.

[7] Priyadarshi P 2015 *Multifidelity multiobjective multidisciplinary design optimization* (M^3DO) *of a semi-ballistic reentry vehicle*. PhD Thesis, IITK, Kanpur, India, December 2015.